coatings

MDPI

Article

Fabrication of Air Conditioning Antimicrobial Filter for Electrically Powered Port Tractors via Electrospinning Coating

Sam-Ki Yoon [1,*], Lyong-Oon Pahn [2], Jeong-Jong Kyun [3] and Soon-Hwan Cho [2,*]

[1] Department of Smart Electrics Automobile, Jeonbuk Campus of Korea Polytechnic, Gimje-si 54352, Jeollabuk-do, Republic of Korea
[2] ENPLUS Co., Ltd., Baeksan-myeon, Gimje-si 54352, Jeollabuk-do, Republic of Korea; lopahn@en3.co.kr
[3] Bukeong Hightech Co., Ltd., Gunsan-si 54001, Jeollabuk-do, Republic of Korea; jj08k@hanmail.net
* Correspondence: sky596072@hanmail.net (S.-K.Y.); chodream@en3.co.kr (S.-H.C.)

Abstract: With the stricter emission regulations for internal combustion engines, electric vehicles, including electrically powered port tractors, have received increasing attention. However, currently, most of the filters used in electric vehicles are conventional membranes that only have the function of filtering particles and foreign objects. Therefore, in order to improve the above issues, the surface of commercial non-woven filter membranes was coated with Ag nanopowder nanofibers and $AgNO_3$ nanofibers via electrospinning. At present, the comparative research on the antibacterial ability of Ag nanopowder and $AgNO_3$ is still blank in the same research system, especially with the use of electrospun coating technology. The morphologies and structures of non-woven fabrics and electrospinning coated samples were characterized by transmission electron microscopy (TEM), scanning electron microscopy (SEM), X-ray diffraction (XRD), and Fourier transform infrared spectroscopy (FTIR). The characterization results indicate that both pure PVA and PVA composite fibers can be successfully coated on the surface of non-woven fabrics. The average diameter of all electrospun PVA composite fibers is distributed in the range of 470–700 nm. The PVA nanofibers with a low content of 1 wt% $AgNO_3$ have good antibacterial properties against *Escherichia coli* (*E. coli*) and *Staphylococcus aureus* (*S. aureus*), with clearance clear zones of inhibition of 26.00 mm and 17.30 mm, respectively.

Keywords: electrically powered port tractors; air conditioning filters; electrospinning; silver nanopowder; silver nitrate

check for updates

Citation: Yoon, S.-K.; Pahn, L.-O.; Kyun, J.-J.; Cho, S.-H. Fabrication of Air Conditioning Antimicrobial Filter for Electrically Powered Port Tractors via Electrospinning Coating. *Coatings* **2024**, *14*, 180. https://doi.org/10.3390/coatings14020180

Academic Editor: Simona Liliana Iconaru

Received: 6 January 2024
Revised: 26 January 2024
Accepted: 30 January 2024
Published: 31 January 2024

Copyright: © 2024 by the authors. Licensee MDPI, Basel, Switzerland. This article is an open access article distributed under the terms and conditions of the Creative Commons Attribution (CC BY) license (https://creativecommons.org/licenses/by/4.0/).

1. Introduction

With the rapid development of the economy, people are increasingly concerned about the quality of the surrounding living environment, especially regarding the various exhaust pollution caused by combustion in internal combustion engines (ICE), such as nitrogen oxides (NO_x), particulate matter (PM), and noise pollution [1,2]. Driven by increasingly stringent exhaust pollution and emission standards, as well as the rapid development of electrochemical technology [3] and solid oxide fuel cell performance [4,5], electric vehicles (EV) are rapidly replacing ICE. The electrification of ICE has undergone rapid development in recent decades and has been applied to many industries, including private cars, Sport Utility Vehicles (SUVs), taxis, trucks, buses, and port tractors [6]. Especially for electrically powered tractors working in ports, the environment inside their cabs is directly affected by the exhaust emissions of surrounding marine engines and other large port shore diesel engines. Most electrically powered tractors are equipped with air conditioning filters, which are the only barrier to ensure that the air inside the driver's cabin is not polluted. Generally speaking, air conditioning filters are composed of non-woven fabrics and support fabrics, and the filter material is made of nylon series non-woven fiber and nylon mesh woven fiber [7]. This conventional filter only has the function of filtering large particulate matter, and after long-term use, bacteria and odors can occur on the surface or inside,

seriously affecting the environment inside the driver's cab and greatly reducing driving comfort. Therefore, developing inexpensive and antibacterial filter materials can effectively improve the above drawbacks.

Electrospinning, as one of the simplest and most efficient methods for preparing functional nanofibers, has been widely used in the filtration of air and water, as well as high-performance antibacterial materials [8,9]. The principle of electrospinning relies on a high-voltage electric field to pull a conductive spinning solution with a certain viscosity into fine fibers ranging from nanometers (nm) to micrometers (μm) [10]. And fiber membranes with different thicknesses can be obtained through collection plates or a roller. A fiber membrane prepared by electrospinning nanotechnology has advantages such as high porosity, large specific surface area, high fiber fineness and uniformity, and large aspect ratio [11,12]. Therefore, it has many advantages in the directional preparation of functional materials. Especially with its porous and large specific surface area characteristics, it is more conducive to contact between the adsorbent and the adsorbed material, thereby releasing its physical and chemical properties [13].

Lyu et al. [14] showed the advantages and future development status of electrospun membranes in the field of air filtration by reviewing various electrospinning materials. They concluded that a fiber membrane prepared by electrospinning has good filtration performance and low pressure drop for particulate matter such as PM2.5 (small particles with a diameter of less than 2.5 microns), PM10 (small particles with a diameter of less than 10 microns), and bacteria in the air. By adjusting the concentration, flow rate, and voltage of the spinning solution, the formation of a bead structure during the spinning process can be controlled. Fiber membranes with a bead structure have high filtration efficiency and low pressure drop for filtration of PM2.5 in air, which meets the basic requirements of air filters. In particular, the graphene oxide/polyacrylonitrile (GOPAN) composite fiber membranes with a unique olive-like bead-on-string structure prepared by [15] had a high filtration efficiency of 99.97% for PM2.5, and the lower pressure drop was only 8 Pa. Liu et al. [16] prepared different fiber membranes using different polymers, including polyacrylonitrile (PAN), polyvinyl pyrrolidone (PVP), polystyrene (PS), polyvinyl alcohol (PVA), and polypropylene (PP), and compared their filtration efficiency, transmittance, capture rate, and lifespan for PM2.5 capture. They found that nanoscale electrospun membranes have excellent filtering effects and light transmittance. In addition, electrospun membranes have great advantages in preparing antibacterial materials. Usually, bacteria in the air are contained in particles. If conventional air filters do not have antibacterial properties, the bacteria will multiply on the filter after it filters the particles, further polluting the filter and causing a serious decrease in its lifespan. Li et al. [17] reviewed the use of various antibacterial raw materials such as silver, quaternary ammonium salt, chitosan, and some metal oxides, including TiO_2, ZnO, MgO, CaO, Al_2O_3, Ag_2O, and CeO_2, in the preparation of antibacterial films via electrospinning. They pointed out that the antibacterial mechanism of inorganic silver nanoparticles mainly relies on (1) silver nanoparticles directly attacking bacterial cells, leading to loss of activity; (2) the binding of silver with electron donors in biomolecules containing sulfur, oxygen, or nitrogen, leading to the failure of cellular enzymes and proteins; and (3) the oxidative stress of the hydroxyl radical (-OH) and superoxide anion ($O+++++_2^-$) in silver particles, inducing bacterial inactivation. In addition, the metal oxide antibacterial agents mentioned above mainly release metal cations, destroy cell membranes and walls, and ultimately lead to the loss of bacterial activity. Zhao et al. [18] prepared poly (vinyl alcohol) (PVA)/carboxymethyl chitosan (CM-chitosan)/silver nanoparticle (AgNP) composite fiber membranes using conventional electrospinning methods and tested their antibacterial activity against Gram-negative *Escherichia coli*. The research results indicated that chitosan has a certain antibacterial ability, but it is weaker compared to that of fiber membranes containing AgNPs, and the antibacterial ability of fibers containing AgNPs is as high as 98% or more. Moreover, they discussed the impact of AgNPs on cytotoxicity. They pointed out that appropriate concentrations of AgNPs have good antibacterial ability and negligible, minimal cytotoxicity, and antibacte-

rial fiber membranes containing AgNPs are reliable and safe. Yardimci et al. [19] prepared composite antibacterial nanofiber membranes using electrospinning technology by adding silver nitrate ($AgNO_3$) to a polyacrylonitrile (PAN)/polyvinylidene fluoride (PVDF) mixture. They showed that the significant change in $AgNO_3$ concentration from 5 wt% to 20 wt% does not disrupt the fiber structure, and that the 10 wt% $AgNO_3$ concentration has excellent antibacterial properties against *Escherichia coli* (*E. coli*) and *Staphylococcus aureus* (*S. aureus*). Yang et al. [20] first prepared a polyvinyl alcohol (PVA) nanofiber membrane using electrospinning technology, and then treated the fiber membrane with $AgNO_3$ solution using a solvothermal method in ethylene glycol. Finally, an antibacterial membrane with an antibacterial rate of over 98% was successfully prepared.

In summary, by reviewing the above literature on the preparation of antibacterial materials, it was found that almost all previous studies used electrospinning technology to directly prepare antibacterial fiber membranes by adding silver nanoparticles or silver nitrate or other antibacterial agents. However, there is a paucity of literature on improving the antibacterial performance of existing filter membranes using electrospinning coating technology. The antibacterial activity and antibacterial mechanism of Ag nanopowder and $AgNO_3$ have never been compared and investigated in the same experimental system. Therefore, in this study, unlike in previous studies, electrospinning technology was employed to coat antibacterial nanofibers (Ag nanopowder and $AgNO_3$) on the surface of commercial non-woven fabrics used in electric port tractors. The antibacterial mechanism of Ag nanopowder and $AgNO_3$ was also thoroughly investigated. The research results indicate that the coating PVA fiber containing a low 1 wt% content of $AgNO_3$ has high antibacterial activity; thus, it has good economic value in replacing expensive Ag nanopowders. In addition, simple electrospinning coating technology can promote the functionalization of the original non-woven fabric membrane, which has great application prospects in the field of preparing functional filter membranes in the future.

2. Materials and Methods

2.1. Experimental Materials

As antibacterial raw materials, silver nanopowder (particle diameter distribution between 80 and 100 nm) and silver nitrate crystal ($AgNO_3$, white crystal, purity $\geq$ 99.0%) were purchased from Green Resource Co., Ltd. (Incheon, Republic of Korea) and Sigma Aldrich (St. Louis, MO, USA), respectively. Polyvinyl alcohol (PVA), as a polymer fiber carrier for antibacterial agents, was purchased from Daejung Chemicals & Metals Co., Ltd., Siheung-si, Republic of Korea. Purified water (conductivity: Max. 2.0 μs/cm; resistivity: Min. 0.5 MΩ) for dissolving PVA was purchased from Samchun Pure Chemical Co., Ltd., Pyeongtaek-si, Republic of Korea. The initial bacterial solutions used to test the antibacterial performance of the filter membranes, including Gram-negative bacterium *Escherichia coli* (*E. coli*) and Gram-positive *Staphylococcus aureus* (*S. aureus*), were purchased from Biozoa Biological Supply Co., Ltd., Seoul, Republic of Korea. All the above reagents were used as received without further purification.

2.2. Preparation of Antibacterial Membranes

Firstly, the 10 wt% PVA solutions were prepared by dissolving PVA powders in purified water and stirring at 60 °C for 12 h. Then, after the PVA powders were completely dissolved in purified water, 1 wt% and 2 wt% Ag nanopowder and $AgNO_3$ crystal were added to the PVA solutions and stirred at 60 °C for 4 h. In order to improve the uniformity of the distribution of AgNP in the PVA solutions, the PVA composite solutions were treated with ultrasound for 2 h. The final prepared spinning solutions were drawn into nanofibers in the electrospinning system shown in Figure 1 and then coated onto the surface of the non-woven fabric after drying and UV treatment. The electrospinning coating time was 2 h. As the main spinning parameters, the high voltage, distance from the needle to the collection roller, and feed rate were 15 kV, 15 cm, and 1 mL/min, respectively. The prepared fiber membranes were vacuum dried for 1 h at 100 °C. For the convenience of statistics

and analysis of some experimental data, untreated raw non-woven fabrics were denoted as M1; non-woven fabrics only coated with PVA fibers were denoted as M2; those that were coated with 1 wt% and 2 wt% Ag nanopowders were denoted as M3 and M4, respectively; and those that were coated with 1 wt% and 2 wt% $AgNO_3$ were denoted as M5 and M6, respectively.

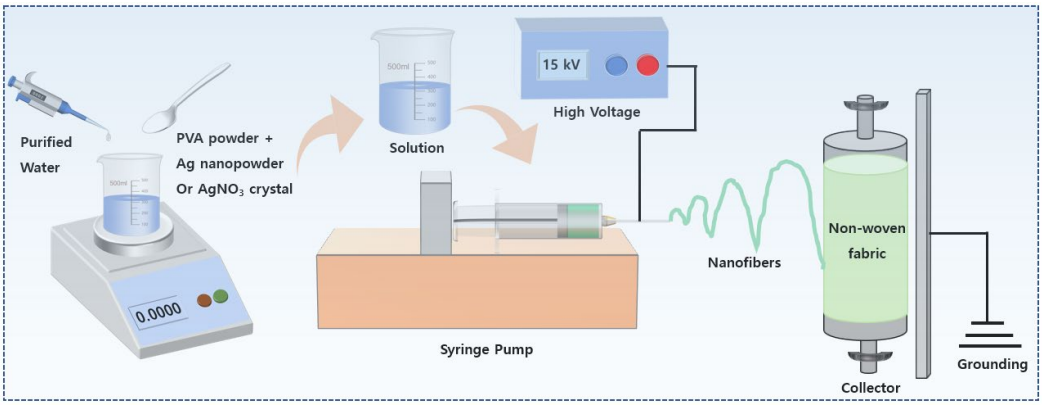

Figure 1. Schematic diagram of the coating system using electrospinning technology.

2.3. Characterization Method

The surface morphology and elemental composition of non-woven fabrics and their coated samples were analyzed by field-emission scanning electron microscope (FE-SEM, Supra-40VP, Carl Zeiss, Jena, Germany. Resolution: 1.0 nm @ 15 kV; 2.0 nm @ 30 kV (VP)) equipped with energy-dispersive X-ray spectroscopy (EDX, Supra-40VP, Carl Zeiss, Germany). Fifty random fibers at different positions in the same SEM image were used to test the average diameter distribution of fibers using the National Institutes of Health (NIH) ImageJ 1.48v software. To observe the distribution of AgNP on PVA fibers more clearly, these samples were analyzed by biological transmission electron microscopy (Bio-TEM, Hitachi, H-7650, Tokyo, Japan). The phase compositions of all samples including antibacterial powder were detected by powder X-ray diffraction (XRD, Bruker D8 Advance, Karlsruhe, Germany) with Cu Kα radiation (λ = 0.15418 nm). The internal bonding architecture of all membranes was analyzed via Fourier transform infrared spectroscopy (FTIR, Perkin Elmer Co., Waltham, MA, USA) with a scanning range of 400–4000 cm^{-1} and a resolution of 1 cm^{-1}.

2.4. Antibacterial Activity Experiment

In this study, *Escherichia coli* (*E. coli*) and *Staphylococcus aureus* (*S. aureus*) were used for the antibacterial activity test. Before starting to test the antibacterial properties of the membranes, all samples were subjected to UV treatment for 2 h on a clean bench. Then, a series of samples with a size of 10 × 25 cm were cut from the prepared fiber membranes using sterile scissors. The cut samples were lightly pressed onto the surface of agar medium inoculated with bacteria to ensure close contact with the agar surface and incubated for 24 h at 37 °C in a constant-temperature incubator. According to the disk diffusion test method, the analysis of antibacterial ability is achieved by measuring the zone of inhibition (clear zone) as shown in Figure 2. An evaluation of antibacterial ability is then made using the following equation:

$$W = (T - D)/2$$

where W (mm) is the width of the clear zone, T (mm) is the total width of the test sample and clear zone, and D (mm) is the width of the test sample.

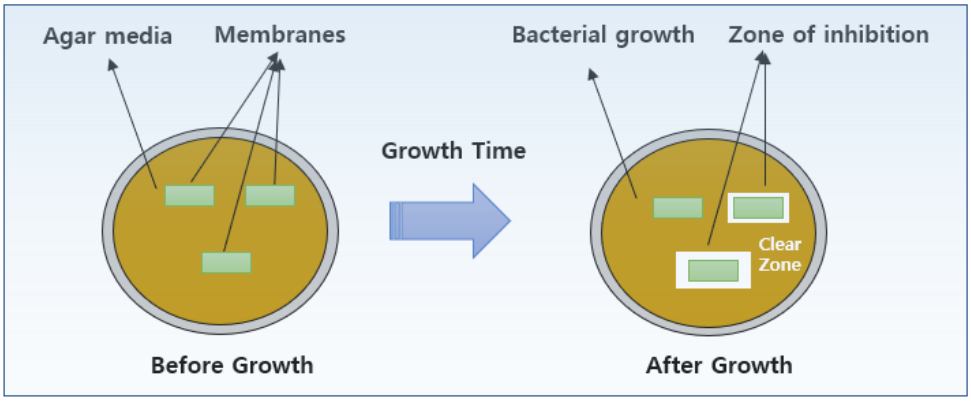

Figure 2. Schematic diagram of the antibacterial activity testing method.

3. Results and Discussion

3.1. Morphology and Structure

Figure 3 shows the TEM images of the pure PVA fiber (M2), PVA fibers with 1 wt% AgNP (M3), and PVA fibers with 1 wt% $AgNO_3$ (M5). As shown in Figure 3, the PVA fibers and the PVA/AgNP and PVA/$AgNO_3$ mixed fibers all exhibited smooth surfaces. In Figure 3b, it is shown that a small amount of silver nanoparticles was loaded onto PVA nanofibers, with a measured particle diameter of 15 nm. In Figure 3c, it is shown that a large number of silver nanoparticles with a diameter of approximately 1–3 nm were loaded onto PVA nanofibers. In addition, it can be observed that silver nanoparticles are uniformly distributed between the mats without significant aggregation, indicating that silver nanoparticles were successfully electrospun into the PVA nanofibers. By comparing their TEM images, it can be proven that silver nanoparticles were successfully incorporated into PVA nanofibers. This is consistent with other findings [21]. The uniform dispersion of silver nanoparticles on nanofibers is of great help in improving antibacterial activity.

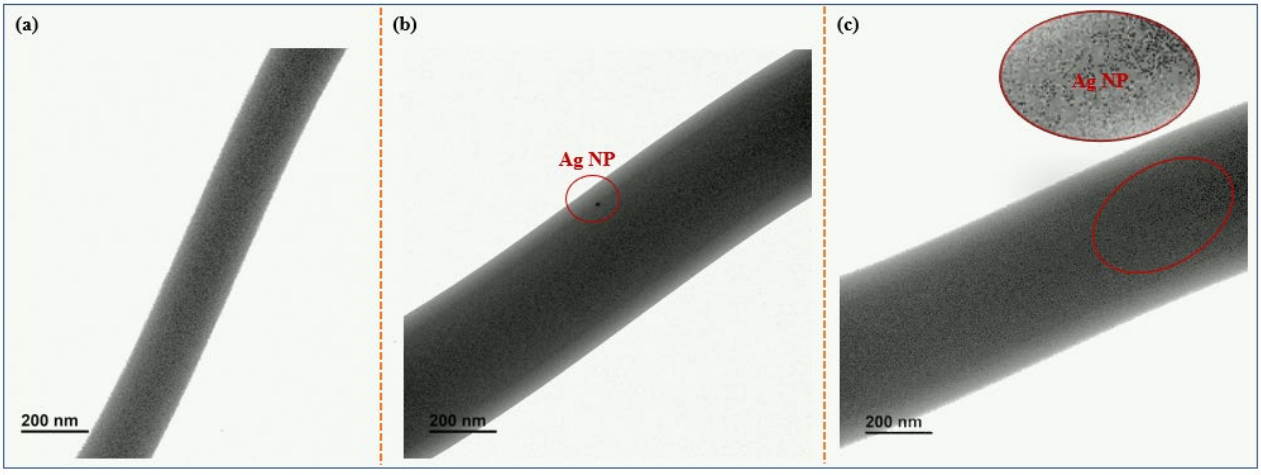

Figure 3. TEM images of the composite fibers: (**a**) M2, (**b**) M3, (**c**) M5. M2: coating with pure PVA fibers; M3: coating with pure 1 wt% Ag nanopowder; M5: coating with pure 1 wt% $AgNO_3$.

Figure 4 shows SEM images of the untreated raw non-woven fabric and its coating membranes. As shown in Figure 4a, the diameter of the non-woven fibers is relatively large, the diameter distribution is uneven, and the pores formed between fibers are also large. However, the diameter distribution of electrospun PVA fibers and composite fibers is relatively uniform, and the surface is smoother. In addition, it can be clearly seen that PVA fibers are arranged in a cross pattern and loaded on the surface of non-woven fibers, indicating that PVA fibers and composite fibers were successfully coated onto the non-woven filter membrane through electrospinning technology. Moreover, no beads appeared

on any of the electrospun PVA fibers, indicating that the PVA solution concentration and operating parameters selected in this experiment are reasonable [22]. By randomly measuring the diameters of 50 fibers, it was found that the average diameters for M1, M2, M3, M4, M5, and M6 were 1.17 µm, 474.58 nm, 559.70 nm, 673.28 nm, 557.36 nm, and 524.08 nm, respectively. Their specific diameter distributions were analyzed by measuring the fiber diameters in the SEM images. The diameter of electrospun fibers is mainly determined by various parameters of electrospinning, such as spinning solution parameters, including the viscosity, conductivity, molecular weight, and surface tension; operational parameters, including the voltage intensity, distance from the needle to the collection plate, and feeding or flow rate; and surrounding environmental factors, including temperature and humidity [10]. Their specific diameter distributions are shown in Figure 5. For electrospun nanofibers, the average diameter of pure PVA fibers was the smallest, while the average diameter increased with the addition of AgNP and $AgNO_3$. Moreover, the addition of AgNP resulted in a larger average diameter of PVA fibers than did the addition of $AgNO_3$. This is because the addition of AgNP and $AgNO_3$ leads to an increase in the concentration of the spinning solution, making it difficult the spinning solution to be pulled into finer fibers under the same high voltage. Other researchers have also reported similar results [23,24].

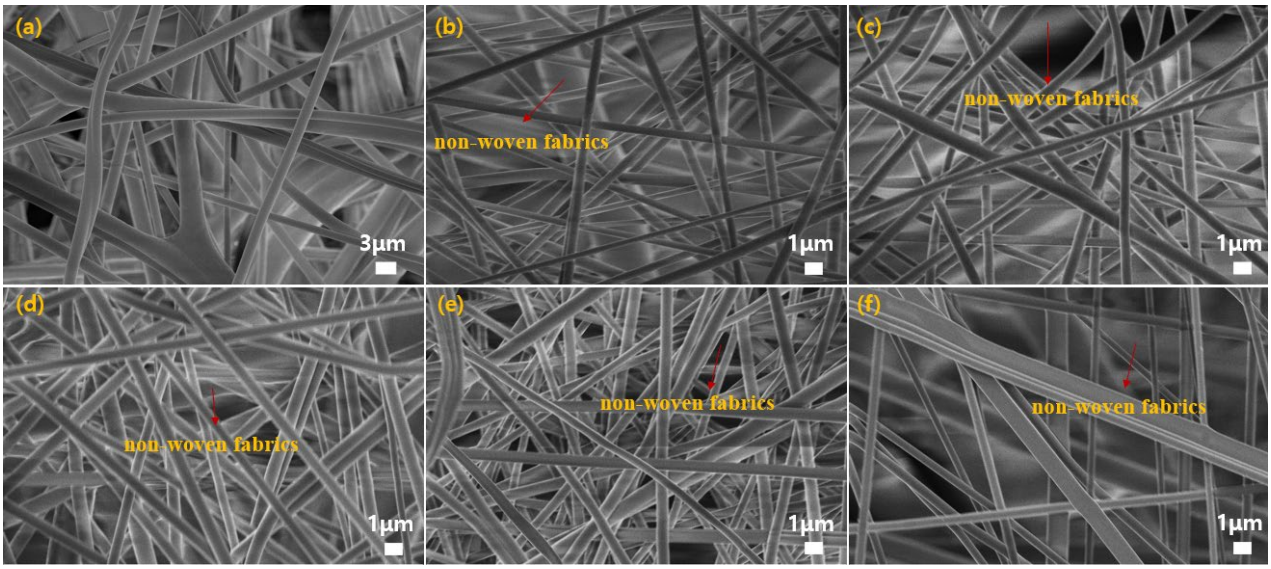

Figure 4. SEM images of the composite fibers: (**a**) M1, (**b**) M2, (**c**) M3, (**d**) M4, (**e**) M5, (**f**) M6. M1: raw non-woven fabric; M2: coating with pure PVA fibers; M3: coating with pure 1 wt% Ag nanopowder; M4: coating with pure 2 wt% Ag nanopowder; M5: coating with pure 1 wt% $AgNO_3$; M6: coating with pure 2 wt% $AgNO_3$.

3.2. X-ray Diffraction (XRD) and Fourier Transform Infrared Spectroscopy (FT-IR)

The chemical elements and composition on the surface of non-woven fabrics coated with PVA, PVA/AgNP, and PVA/$AgNO_3$ mixed fibers undergo certain changes. In order to investigate the changes in the internal chemical structure, all samples were examined by XRD and FTIR.

Figure 6 shows the XRD patterns of untreated raw non-woven fabrics and their coating membranes. For M1, the non-woven fibers have four typical peaks: the peaks at $2\theta = 21.7°$, 18.5°, 16.8°, and 14.07° contribute to the (111), (130), (040), and (110) planes [25]. On the other hand, the peak positions observed in PVA and PVA composite fibers are approximately those observed in non-woven fabrics. This is because only one hour of PVA coating resulted in a thin film, which cannot cover the peak strength of the non-woven fiber materials in XRD testing. In addition, the peak for PVA and PVA composite film shows a slight shift to the left at $2\theta = 21.7°$, which can be attributed to the interaction

between the (101) plane of the semi crystalline structure of PVA fiber and the (111) plane of the non-woven fabric. Moreover, the characteristic peaks at 2θ = 42.3° for M3–M6 confirm that Ag nanoparticles are present on the surface of the PVA composite film. Other researchers [26–28] have also pointed out that the peak for Ag nanostructures is between 40° and 45°.

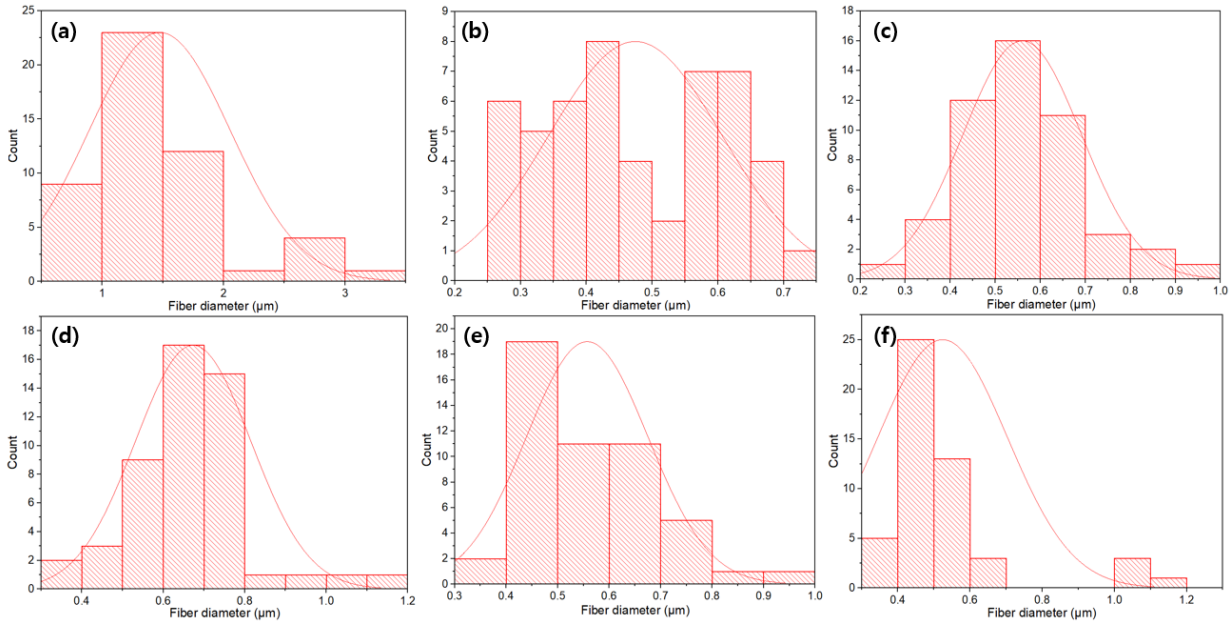

Figure 5. Fiber diameter distribution of (**a**) M1, (**b**) M2, (**c**) M3, (**d**) M4, (**e**) M5, (**f**) M6. M1: raw non-woven fabric; M2: coating with pure PVA fibers; M3: coating with pure 1 wt% Ag nanopowder; M4: coating with pure 2 wt% Ag nanopowder; M5: coating with pure 1 wt% $AgNO_3$; M6: coating with pure 2 wt% $AgNO_3$.

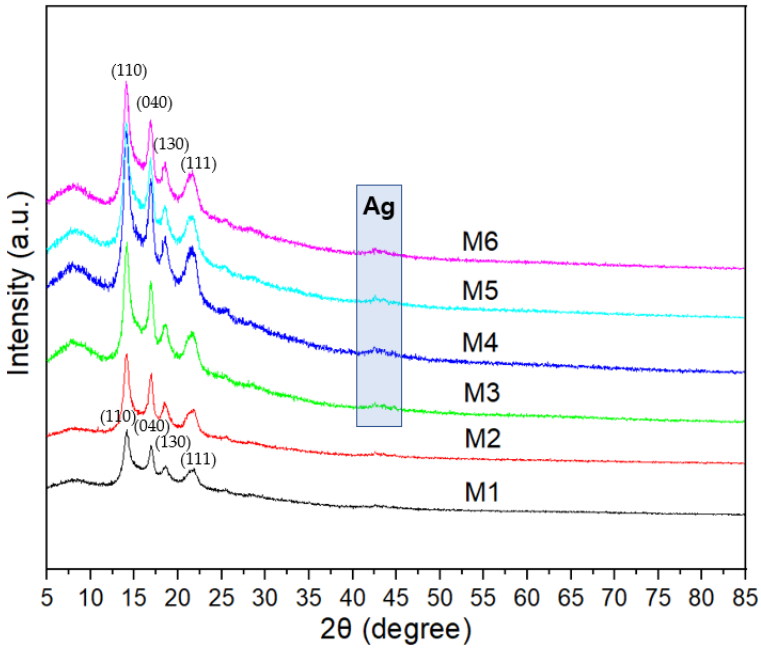

Figure 6. XRD spectra of M1, M2, M3, M4, M5, and M6. M1: raw non-woven fabric; M2: coating with pure PVA fibers; M3: coating with pure 1 wt% Ag nanopowder; M4: coating with pure 2 wt% Ag nanopowder; M5: coating with pure 1 wt% $AgNO_3$; M6: coating with pure 2 wt% $AgNO_3$.

Figure 7 shows the FTIR spectra of untreated raw non-woven fabrics and their coating membranes. For the raw non-woven fabrics, there are several bands characteristic of PP structure, such as the absorption peaks around 3000 cm^{-1}, contributed by C–H stretching vibrations in PP chains, and the absorption peaks at about 1457 cm^{-1} and 1380 cm^{-1}, arising from -CH_2 and -CH_3 bending vibrations, respectively [29]. When comparing the pure PVA and mixed PVA fibers to the non-woven fabrics, some new absorption peaks were observed in M2, M3, M4, M5, and M6. The strong absorption peak around 3300 cm^{-1} corresponds to the vibrations of O–H stretching from H bonds. The bands at 1733 cm^{-1} correspond to C=C stretching vibration. The peak at 1094 cm^{-1} corresponds to C–O stretching of the acetyl group present on the PVA backbone [30]. The peak around 1257 cm^{-1} is assigned to -CH wagging vibration [31]. The peak around 608 cm^{-1} is assigned to OH stretching vibration [31]. In addition, as AgNP and $AgNO_3$ was added to the PVA solution, the intensity of these typical peaks was enhanced. Especially at around 1380 cm^{-1}, the intensity of the peak was significantly enhanced due to the combined effect of Ag and -OH bonding interaction. The above phenomena indicate that pure PVA and PVA/AgNP and PVA/$AgNO_3$ mixed fibers were successfully coated onto the surface of the non-woven fabrics.

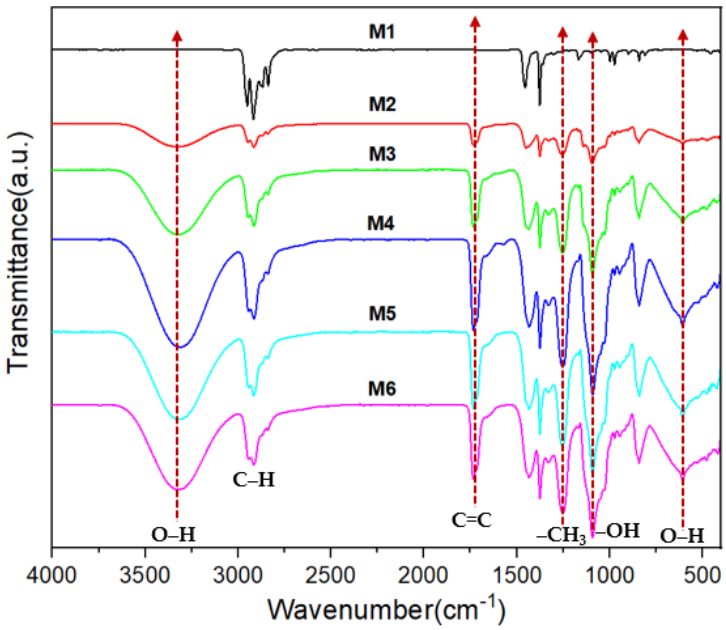

Figure 7. FTIR spectra of M1, M2, M3, M4, M5, and M6. M1: raw non-woven fabric; M2: coating with pure PVA fibers; M3: coating with pure 1 wt% Ag nanopowder; M4: coating with pure 2 wt% Ag nanopowder; M5: coating with pure 1 wt% $AgNO_3$; M6: coating with pure 2 wt% $AgNO_3$.

3.3. Antibacterial Activity

Figure 8 shows the antibacterial efficacy of M1 (non-woven fabric), M2 (non-woven fabric coated with pure PVA fibers), M3 (non-woven fabric coated with PVA fibers and 1 wt% AgNP), M4 (non-woven fabric coated with PVA fibers and 2 wt% AgNP), M5 (non-woven fabric coated with PVA fibers and 1 wt% $AgNO_3$), and M6 (non-woven fabric coated with PVA fibers and 2 wt% $AgNO_3$) against both Gram-negative *Escherichia coli* (*E. coli*) and Gram-positive *Staphylococcus aureus* (*S. aureus*). As shown in the figure, there was no clear zone of inhibition around M1–M4. That is to say, pure non-woven fabrics and non-woven fabrics coated with pure PVC fibers had no antibacterial activity against both *E. coli* and *S. aureus*. Even M3 and M4, respectively coated with 1% and 2% AgNP, did not exhibit antibacterial activity. Only M5 had certain antibacterial ability against both *E. coli* and *S. aureus*, as clear zones of different sizes appeared around it. Moreover, sample M6 only had antibacterial activity against *E. coli*. According to the equation for antibacterial ability, as shown in Figure 9, the widths of the clear zones for

M5 on *E. coli* and *S. aureus* were calculated to be 26.00 mm and 17.30 mm, respectively, while the width of the clear zone for M6 on *E. coli* was calculated to be 8.30 mm. The above results indicate that even low concentrations (1 wt%) of $AgNO_3$ could be used to prepare functional fiber membranes with excellent antibacterial properties through electrospun coating technology. In addition, although both Ag nanopowder and $AgNO_3$ crystal contain silver ions, the antibacterial properties of the fiber membranes prepared by electrospinning differ greatly. This may be because the viscosity and conductivity of the electrospinning precursors prepared by mixing Ag nanopowder and $AgNO_3$ with PVA solution are different, resulting in different distribution characteristics of silver nanoparticles on PVA nanofibers during the electrospinning process. That is, the smaller the diameter of PVA nanofibers, and the more silver nanoparticles are located on the surface of the fibers, the better the antibacterial activity.

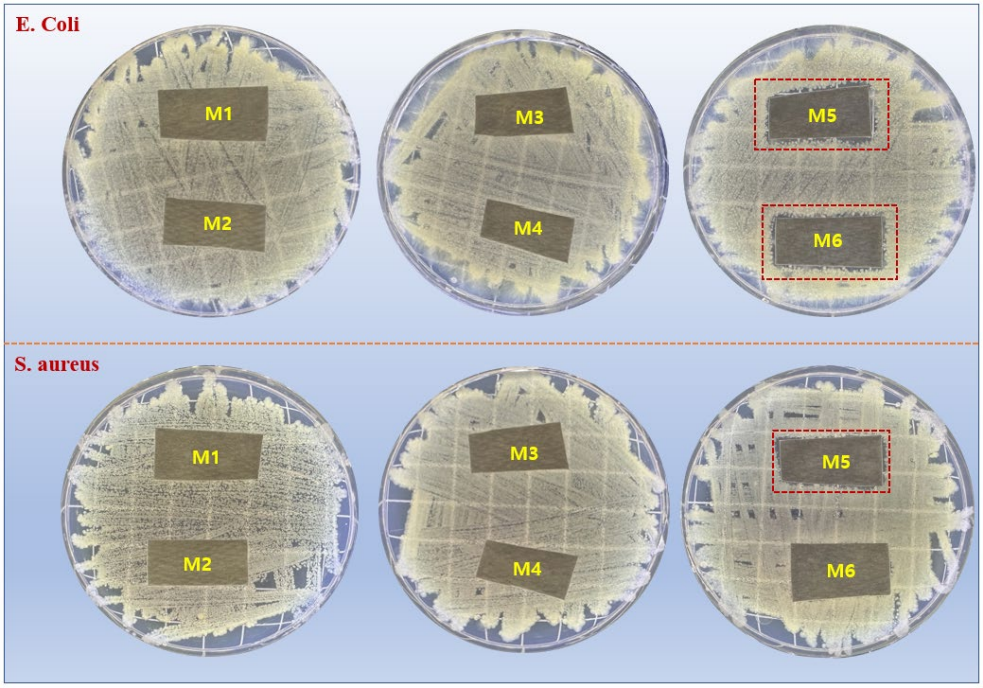

Figure 8. Comparison of antibacterial ability of all membranes against *Escherichia coli* and *Staphylococcus aureus*. M1: raw non-woven fabric; M2: coating with pure PVA fibers; M3: coating with pure 1 wt% Ag nanopowder; M4: coating with pure 2 wt% Ag nanopowder; M5: coating with pure 1 wt% $AgNO_3$; M6: coating with pure 2 wt% $AgNO_3$.

In addition, the antibacterial activity of M5 against Gram-negative *E. coli* was significantly higher than that against Gram-positive *S. aureus*. This is because the peptidoglycan layer of *S. aureus* (+) has a thickness of approximately 20–80 nm, which is thicker than the peptidoglycan layer in *E. coli* (approximately 7–8 nm), forming a barrier that prevents the penetration of silver nanoparticles. Moreover, silver nanoparticles are more likely to adsorb onto negatively charged cell surfaces (i.e., *E. coli*) and interfere with cell permeability. The antibacterial mechanism of silver nanoparticles against *E. coli* and *S. aureus* is mainly due to the entry of silver nanoparticles into cells and their interaction with sulfur- and phosphorus-containing compounds, which disrupt cells by affecting the respiratory chain [32].

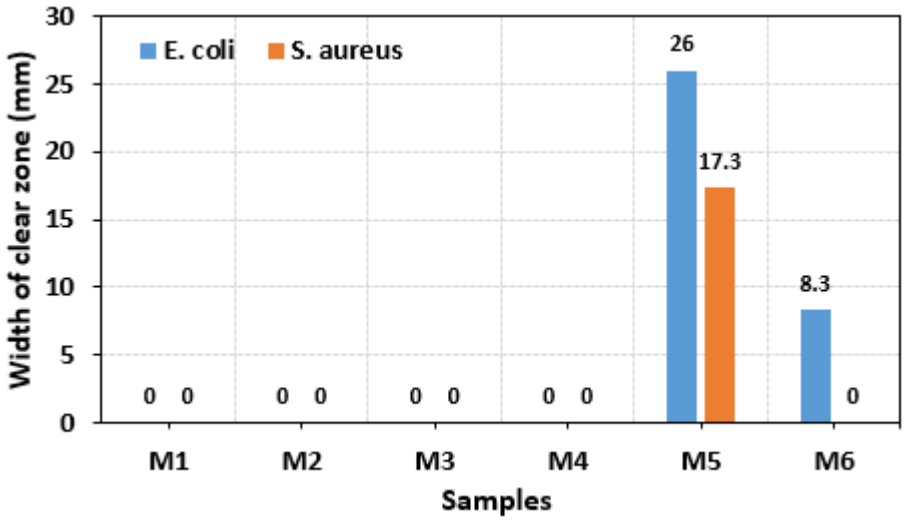

Figure 9. Comparison of the width of the clear zone for all test samples. M1: raw non-woven fabric; M2: coating with pure PVA fibers; M3: coating with pure 1 wt% Ag nanopowder; M4: coating with pure 2 wt% Ag nanopowder; M5: coating with pure 1 wt% $AgNO_3$; M6: coating with pure 2 wt% $AgNO_3$.

To further investigate the antibacterial mechanisms of silver powder (AgNP) and silver nitrate ($AgNO_3$) against *E. coli* and *S. aureus*, 0.002 g samples of AgNP and $AgNO_3$ were placed on the culture media of *E. coli* and *S. aureus*. Their antibacterial activity is shown in Figure 10. As shown in the figure, the clearance zone of inhibition of $AgNO_3$ was slightly larger than that of AgNP. After calculation, the clearance zones of inhibition of AgNP and $AgNO_3$ on *E. coli* were approximately 11.41 mm and 19.39 mm, respectively, and those on *S. aureus* were 11.15 mm and 18.88 mm, respectively. The antibacterial ability of the same antibacterial agent against *E. coli* and *S. aureus* is almost the same, indicating that both AgNP and $AgNO_3$ have high antibacterial activity and do not exhibit different antibacterial activities due to differences in bacterial cell wall thickness. The higher antibacterial activity exhibited by $AgNO_3$ than by AgNP can be attributed to the presence of Ag ions in $AgNO_3$. Interaction with Ag ions can directly destroy the bacterial cell wall and cause bacterial inactivation, while AgNP undergoes oxidation before interacting with the cell wall, which may lead to the disappearance of some antibacterial activity during the oxidation process. This is consistent with the report in [33].

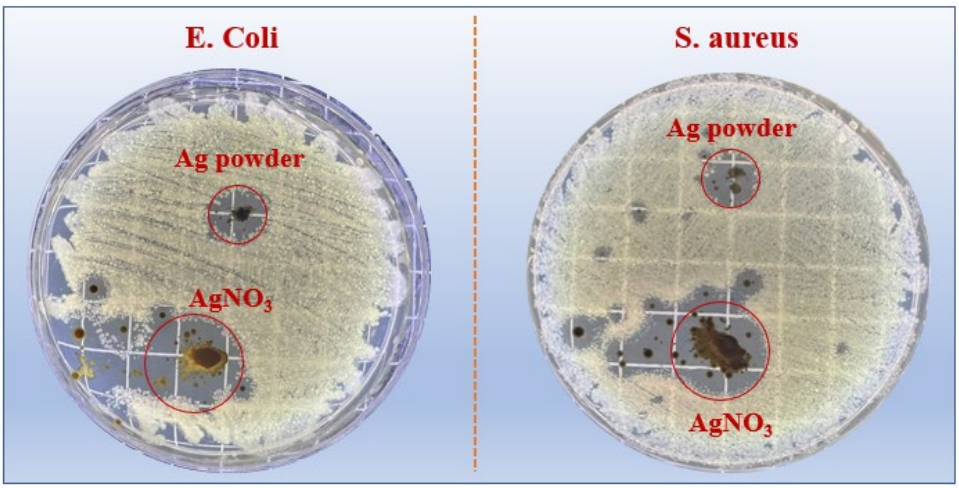

Figure 10. Comparison of the antibacterial ability of AgNP and $AgNO_3$ against *Escherichia coli* and *Staphylococcus aureus*.

3.4. Antibacterial Mechanism

Figure 11 shows the cellular structure of *E. coli* and *S. aureus*. *E. coli* and *S. aureus* both belong to the prokaryotes, both containing cellular structures, and their cells do not have formed nuclei. They both contain two types of nucleic acids, DNA and RNA, and only have ribosomes as organelles. Therefore, their ecological commonalities include their cell structure, cell shell (peptidoglycan), nucleoid composed of DNA and proteins, ribosomes, and cell fluid. According to statistics, *E. coli* bacterial cells are typically approximately 2.0 μm long and rod-shaped with a diameter of 0.25–1.0 μm [34]. Cells also display many pili or fimbria, usually extending to the glass surface, but in some cases, they can also be seen on the cell surface. *S. aureus* typically has a nearly spherical structure, approximately 0.5–1.5 μm in diameter, and most cells exist in clusters, with few isolated cells; the texture on the cell surface is very rough [35]. In addition, *E. coli* is a Gram-negative bacterium with a relatively thin peptidoglycan layer of 7–8 nm, compared to that of Gram-positive *S. aureus* (20–80 nm). The function of peptidoglycan is to endow the cell wall with shape and strength. The thickness of the peptidoglycan layer plays an important role in providing a rigid structure that serves as a barrier for chitosan interactions [34,35].

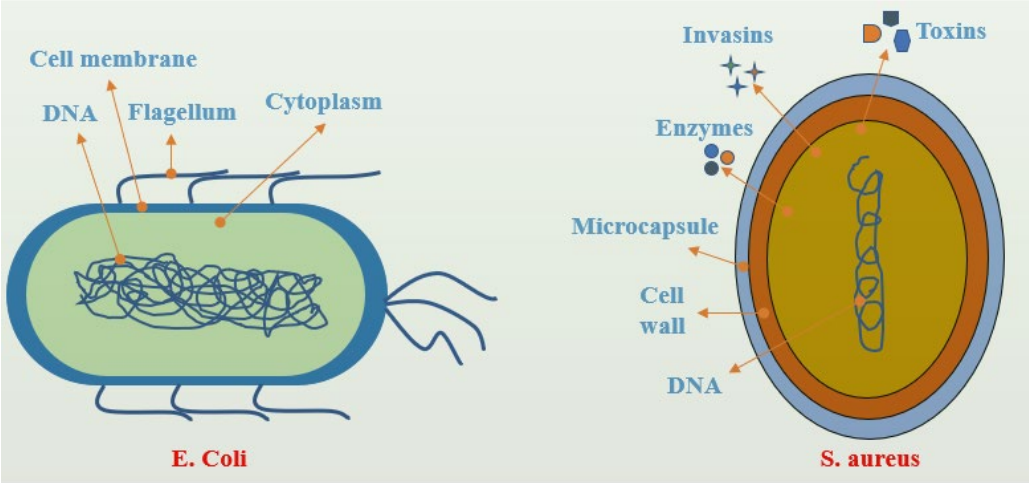

Figure 11. Structural diagram of *E. coli* and *S. aureus*.

Figure 12 shows a schematic diagram of the antibacterial mechanism. The antibacterial mechanisms of silver nanoparticles against *E. coli* and *S. aureus* mainly include the following: (i) silver nanoparticles adsorb on the surface of cell membranes, causing a loss of respiratory and permeability functions of cell membranes; (ii) nanoparticles penetrate into cells and interact with DNA and active enzymes containing phosphorus and sulfur, leading to cell inactivation; (iii) nanoparticles release silver ions to further inhibit cell activity [21]. The cell membrane is a biological membrane that separates the internal and external environment of a cell, which is the most basic barrier to ensure cell activity. The cell membrane is composed of a phospholipid bilayer and embedded proteins. When the cell membrane is damaged, intracellular enzymes leak to the outside of the cell, leading to a significant decrease in cell activity [36]. Therefore, the smaller the size of silver particles, the easier it is for them to adsorb onto the cell membrane and penetrate into the cell interior. In addition, silver nanoparticles have higher antibacterial ability against Gram-negative bacteria (*E. coli*) compared to Gram-positive bacteria (*S. aureus*). Their main contribution is that *E. coli* has a thinner cell membrane and a negative charge, which makes it easy for silver nanoparticles to penetrate the cell and interact with positively charged silver ions [37,38]. In addition, the mechanism of antibacterial activity of silver nanoparticles is also related to the production of reactive oxygen species (ROS), which leads to cellular oxidative stress and apoptosis. The increase in ROS induced by silver nanoparticles depends on the presence of reactive groups such as free radicals or oxidants, as well as the inactivation of ROS protective pathways,

such as glutathione (GSH—a typical cellular antioxidant) damage [39,40]. Moreover, the size, shape, and surface functional groups of silver nanoparticles play an important role in their antibacterial activity. Silver particles with characteristics such as small particle size, non-circular (triangular, prismatic, hexagonal) or sharp (due to with higher charge density) structure, or the presence of *C. inerme* functional groups on the nanoparticle surface often exhibit excellent antibacterial activity [40].

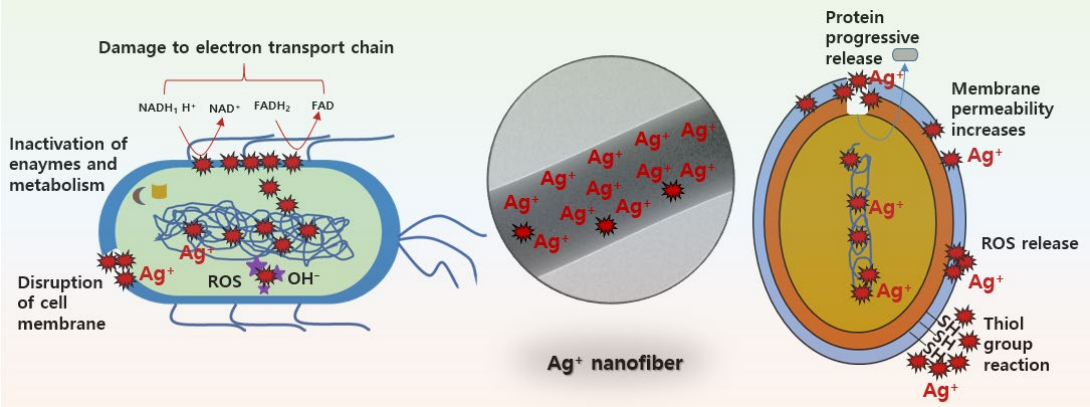

Figure 12. Antibacterial mechanisms.

4. Conclusions

In this study, in order to prepare antibacterial filter membranes for electrically powered port tractors, commercial non-woven fabrics were successfully coated with PVA solutions containing 1 wt% and 2 wt% silver nanopowder (AgNP) and 1 wt% and 2 wt% silver nitrate ($AgNO_3$) via electrospinning technology. The antibacterial activity of non-woven fabrics and coated samples against *Escherichia coli* (*E. coli*) and *Staphylococcus aureus* (*S. aureus*) was compared and investigated. The detailed results are summarized as follows:

i. The average diameter of PVA composite fibers prepared by electrospinning was at the nanometer level, distributed between 470 and 700 nm, which is much smaller than the diameter of the non-woven fibers (1.17 μm).
ii. The characterization results of XRD and FTIR indicate that pure PVA fibers and PVA/AgNP and PVA/$AgNO_3$ composite fibers were successfully coated onto the surface of non-woven fiber membranes using electrospinning technology to prepare functional membranes with antibacterial properties.
iii. By comparing the antibacterial properties, it was found that PVA containing 1 wt% $AgNO_3$ had the best antibacterial properties against *E. coli* and *S. aureus*, with clearance zones of inhibition of 26.00 mm and 17.30 mm, respectively.
iv. The antibacterial mechanism of silver particles against *E. coli* and *S. aureus* is mainly related to their adsorption on the cell membrane, disruption of the cell membrane's integrity, permeation into the cell, and interaction with DNA and proteins.

In future work, we will investigate the filtration performance of these membranes on particles with different diameters (i.e., PM0.8, PM1.0, PM2.5) and finally test their practical application effect and durability in electrically powered port tractors. The antibacterial filter membrane prepared by coating with 1 wt% of $AgNO_3$ has good economic value and great potential for application in the field of filter materials in the future.

Author Contributions: Conceptualization, S.-H.C. and S.-K.Y.; methodology, S.-K.Y.; software, S.-K.Y.; validation, S.-H.C., L.-O.P., J.-J.K. and S.-K.Y.; investigation, S.-H.C., L.-O.P., J.-J.K. and S.-K.Y.; resources, S.-H.C., L.-O.P., J.-J.K. and S.-K.Y.; data curation, S.-H.C. and S.-K.Y.; writing—original draft preparation, S.-H.C.; writing—review and editing, S.-H.C. and S.-K.Y.; supervision, S.-K.Y.; project administration, S.-H.C. and L.-O.P.; funding acquisition, S.-H.C. and L.-O.P. All authors have read and agreed to the published version of the manuscript.

Funding: This research was supported by Korea Institute of Marine Science & Technology Promotion (KIMST) funded by the Ministry of Oceans and Fisheries, Korea (20220583).

Institutional Review Board Statement: Not applicable.

Informed Consent Statement: Not applicable.

Data Availability Statement: Data are contained within the article.

Conflicts of Interest: Author Lyong-Oon Pahn and Soon-Hwan Cho were employed by the company ENPLUS Co., Ltd. Author Jeong-Jong Kyun was employed by the company Bukeong Hightech Co., Ltd. The remaining author declares that the research was conducted in the absence of any commercial or financial relationships that could be construed as a potential conflict of interest.

References

1. Li, C.; Dixit, P.; Welch, B.; Nigam, A.; Soriano, B.; Lee, J.; Russell, R.L.; Jiang, Y.; Zhu, H.; Karavalakis, G.; et al. Yard tractors: Their path to zero emissions. *Transp. Res. Part D Transp. Environ.* **2021**, *98*, 102972. [CrossRef]
2. Fredianelli, L.; Bolognese, M.; Fidecaro, F.; Licitra, G. Classification of noise sources for port area noise mapping. *Environments* **2021**, *8*, 12. [CrossRef]
3. Pahlavani, H.; Shayeh, J.S.; Nouralishahi, A.; Paroushi, M.S. Nano graphene porous/conductive polymer as a composite material for energy storage in supercapacitors. *J. Appl. Polym. Sci.* **2024**, *141*, e54812. [CrossRef]
4. Dizaj, R.B.; Sabahi, N. Optimizing LSM-LSF composite cathodes for enhanced solid oxide fuel cell performance: Material engineering and electrochemical insights. *World J. Adv. Res. Rev.* **2023**, *20*, 1284–1291. [CrossRef]
5. Dizaj, R.B.; Sabahi, N. Laboratory preparation of LSM and LSF sputtering targets using PTFE rings for deposition of SOFC thin film electrodes. *World J. Adv. Eng. Technol. Sci.* **2023**, *10*, 203–212. [CrossRef]
6. Yang, X.; Lin, W.; Gong, R.; Zhu, M.; Springer, C. Transport decarbonization in big cities: An integrated environmental co-benefit analysis of vehicles purchases quota-limit and new energy vehicles promotion policy in Beijing. *Sustain. Cities Soc.* **2021**, *71*, 102976. [CrossRef]
7. Qian, C. The development and property studies of nonwoven filtering materials for car air-conditioner. *Adv. Mater. Res.* **2011**, *322*, 373–376. [CrossRef]
8. Ge, J.C.; Kim, J.Y.; Yoon, S.K.; Choi, N.J. Fabrication of low-cost and high-performance coal fly ash nanofibrous membranes via electrospinning for the control of harmful substances. *Fuel* **2019**, *237*, 236–244. [CrossRef]
9. Ge, J.C.; Choi, N.J. Performance of electrospun nanofibrous membranes for trapping of BTX aromatic hydrocarbons and heavy metal ions: Mechanisms, isotherms and kinetics. *J. Clean. Prod.* **2019**, *217*, 388–397. [CrossRef]
10. Bhardwaj, N.; Kundu, S.C. Electrospinning: A fascinating fiber fabrication technique. *Biotechnol. Adv.* **2010**, *28*, 325–347. [CrossRef]
11. Agarwal, S.; Wendorff, J.H.; Greiner, A. Use of electrospinning technique for biomedical applications. *Polymer* **2008**, *49*, 5603–5621. [CrossRef]
12. Ahmed, F.E.; Lalia, B.S.; Hashaikeh, R. A review on electrospinning for membrane fabrication: Challenges and applications. *Desalination* **2015**, *356*, 15–30. [CrossRef]
13. Ge, J.C.; Wu, G.; Xu, G.; Song, J.H.; Choi, N.J. Synthesis of Polyvinyl Alcohol/Coal Fly Ash Hybrid Nano-Fiber Membranes for Adsorption of Heavy Metals in Diesel Fuel. *Nanomaterials* **2023**, *13*, 1674. [CrossRef]
14. Lyu, C.; Zhao, P.; Xie, J.; Dong, S.; Liu, J.; Rao, C.; Fu, J. Electrospinning of nanofibrous membrane and its applications in air filtration: A review. *Nanomaterials* **2021**, *11*, 1501. [CrossRef]
15. Li, J.; Zhang, D.; Yang, T.; Yang, S.; Yang, X.; Zhu, H. Nanofibrous membrane of graphene oxide-in-polyacrylonitrile composite with low filtration resistance for the effective capture of $PM_{2.5}$. *J. Membr. Sci.* **2018**, *551*, 85–92. [CrossRef]
16. Liu, C.; Hsu, P.-C.; Lee, H.-W.; Ye, M.; Zheng, G.; Liu, N.; Li, W.; Cui, Y. Transparent air filter for high-efficiency $PM_{2.5}$ capture. *Nat. Commun.* **2015**, *6*, 6205. [CrossRef]
17. Li, H.; Chen, X.; Lu, W.; Wang, J.; Xu, Y.; Guo, Y. Application of electrospinning in antibacterial field. *Nanomaterials* **2021**, *11*, 1822. [CrossRef] [PubMed]
18. Zhao, Y.; Zhou, Y.; Wu, X.; Wang, L.; Xu, L.; Wei, S. A facile method for electrospinning of Ag nanoparticles/poly (vinyl alcohol)/carboxymethyl-chitosan nanofibers. *Appl. Surf. Sci.* **2012**, *258*, 8867–8873. [CrossRef]
19. Ince Yardimci, A.; Durmus, A.; Kayhan, M.; Tarhan, O. Antibacterial Activity of $AgNO_3$ Incorporated Polyacrylonitrile/Polyvinylidene Fluoride (PAN/PVDF) Electrospun Nanofibrous Membranes and Their Air Permeability Properties. *J. Macromol. Sci. Part B* **2022**, *61*, 749–762. [CrossRef]
20. Yang, Y.; Zhang, Z.; Wan, M.; Wang, Z.; Zou, X.; Zhao, Y.; Sun, L. A facile method for the fabrication of silver nanoparticles surface decorated polyvinyl alcohol electrospun nanofibers and controllable antibacterial activities. *Polymers* **2020**, *12*, 2486. [CrossRef] [PubMed]
21. Zhang, Z.; Wu, Y.; Wang, Z.; Zhang, X.; Zhao, Y.; Sun, L. Electrospinning of Ag Nanowires/polyvinyl alcohol hybrid nanofibers for their antibacterial properties. *Mater. Sci. Eng. C* **2017**, *78*, 706–714. [CrossRef]
22. Ge, J.C.; Wu, G.; Yoon, S.K.; Kim, M.S.; Choi, N.J. Study on the preparation and lipophilic properties of polyvinyl alcohol (PVA) nanofiber membranes via green electrospinning. *Nanomaterials* **2021**, *11*, 2514. [CrossRef]

23. Zhang, Z.; Wu, Y.; Wang, Z.; Zou, X.; Zhao, Y.; Sun, L. Fabrication of silver nanoparticles embedded into polyvinyl alcohol (Ag/PVA) composite nanofibrous films through electrospinning for antibacterial and surface-enhanced Raman scattering (SERS) activities. *Mater. Sci. Eng. C* **2016**, *69*, 462–469. [CrossRef] [PubMed]
24. Jin, W.-J.; Jeon, H.J.; Kim, J.H.; Youk, J.H. A study on the preparation of poly(vinyl alcohol) nanofibers containing silver nanoparticles. *Synth. Met.* **2007**, *157*, 454–459. [CrossRef]
25. Malakhov, S.N.; Dmitryakov, P.V.; Pichkur, E.B.; Chvalun, S.N. Nonwoven materials produced by melt electrospinning of polypropylene filled with calcium carbonate. *Polymers* **2020**, *12*, 2981. [CrossRef] [PubMed]
26. Hang, A.T.; Tae, B.; Park, J.S. Non-woven mats of poly(vinyl alcohol)/chitosan blends containing silver nanoparticles: Fabrication and characterization. *Carbohydr. Polym.* **2010**, *82*, 472–479. [CrossRef]
27. Amirjani, A.; Kamani, P.; Hosseini, H.R.M.; Sadrnezhaad, S.K. SPR-based assay kit for rapid determination of Pb^{2+}. *Anal. Chim. Acta* **2022**, *1220*, 340030. [CrossRef] [PubMed]
28. Amirjani, A.; Salehi, K.; Sadrnezhaad, S.K. Simple SPR-based colorimetric sensor to differentiate Mg^{2+} and Ca^{2+} in aqueous solutions. *Spectrochim. Acta Part A Mol. Biomol. Spectrosc.* **2022**, *268*, 120692. [CrossRef]
29. Gorade, V.G.; Chaudhary, B.U.; Kale, R.D. Moisture management of polypropylene non-woven fabric using microcrystalline cellulose through surface modification. *Appl. Surf. Sci. Adv.* **2021**, *6*, 100151. [CrossRef]
30. Bhajantri, R.F.; Ravindrachary, V.; Harisha, A.; Crasta, V.; Nayak, S.P.; Poojary, B. Microstructural studies on $BaCl_2$ doped poly(vinyl alcohol). *Polymer* **2006**, *47*, 3591–3598. [CrossRef]
31. Hebbar, V.; Bhajantri, R.; Naik, J.; Rathod, S.G. Thiazole yellow G dyed PVA films for optoelectronics: Microstructural, thermal and photophysical studies. *Mater. Res. Express* **2016**, *3*, 075301. [CrossRef]
32. Cheng, T.-H.; Lin, S.-B.; Chen, L.-C.; Chen, H.-H. Studies of the antimicrobial ability and silver ions migration from silver nitrate-incorporated electrospun nylon nanofibers. *Food Packag. Shelf Life* **2018**, *16*, 129–137. [CrossRef]
33. Jiraroj, D.; Tungasmita, S.; Tungasmita, D.N. Silver ions and silver nanoparticles in zeolite A composites for antibacterial activity. *Powder Technol.* **2014**, *264*, 418–422. [CrossRef]
34. Yusuf, Y.; Ghazali, M.J.; Otsuka, Y.; Ohnuma, K.; Morakul, S.; Nakamura, S.; Abdollah, M.F. Antibacterial properties of laser surface-textured TiO_2/ZnO ceramic coatings. *Ceram. Int.* **2020**, *46*, 3949–3959. [CrossRef]
35. Fayisa, W.O.; Tuli, N.F. Review on *Staphylococcus aureus*. *Int. J. Nurs. Care Res.* **2023**, *1*, 1–8.
36. Shen, S.; Zhang, T.; Yuan, Y.; Lin, S.; Xu, J.; Ye, H. Effects of cinnamaldehyde on *Escherichia coli* and *Staphylococcus aureus* membrane. *Food Control* **2015**, *47*, 196–202. [CrossRef]
37. Liao, C.; Li, Y.; Tjong, S.C. Bactericidal and cytotoxic properties of silver nanoparticles. *Int. J. Mol. Sci.* **2019**, *20*, 449. [CrossRef]
38. Fröhlich, E.E.; Fröhlich, E. Cytotoxicity of nanoparticles contained in food on intestinal cells and the gut microbiota. *Int. J. Mol. Sci.* **2016**, *17*, 509. [CrossRef]
39. Abdal Dayem, A.; Hossain, M.K.; Lee, S.B.; Kim, K.; Saha, S.K.; Yang, G.-M.; Choi, H.Y.; Cho, S.-G. The role of reactive oxygen species (ROS) in the biological activities of metallic nanoparticles. *Int. J. Mol. Sci.* **2017**, *18*, 120. [CrossRef]
40. Ramalingam, B.; Parandhaman, T.; Das, S.K. Antibacterial effects of biosynthesized silver nanoparticles on surface ultrastructure and nanomechanical properties of gram-negative bacteria viz. *Escherichia coli* and *Pseudomonas aeruginosa*. *ACS Appl. Mater. Interfaces* **2016**, *8*, 4963–4976.

Disclaimer/Publisher's Note: The statements, opinions and data contained in all publications are solely those of the individual author(s) and contributor(s) and not of MDPI and/or the editor(s). MDPI and/or the editor(s) disclaim responsibility for any injury to people or property resulting from any ideas, methods, instructions or products referred to in the content.